A numerical approach for a system of transport equations in the field of radiotherapy

Teddy Pichard [1,*], Stéphane Brull[2], Bruno Dubroca[3]

[1] *Sorbonne Universités, UPMC Univ Paris 06, UMR 7598, Laboratoire Jacques-Louis Lions, 4 place Jussieu, F-75005, Paris, France.*
[2] *INP Bordeaux, UMR 5251, Institut de Mathématiques de Bordeaux, 351 cours de la libération, F-33400, Talence, France.*
[3] *Université de Bordeaux, UMR 5801, Laboratoire des Composites Thermostructuraux, 3 allée de la Boétie, F-33600, Pessac, France.*

Abstract. Numerical schemes for systems of transport equations are commonly constrained by a stability condition of Courant-Friedrichs-Lewy (CFL) type. A system modeling the steady transport of photons and electrons in the field of radiotherapy is considered. Naive discretizations of such a system are commonly constrained by a very restrictive CFL conditions. This issue is circumvented by constructing an implicit scheme based on a relaxation approach.
An entropy-based moment model, namely the M_1 model, is considered. The M_1 system of equations possesses the non-linear flux terms of an hyperbolic system but no time derivative. The flux terms are well-defined only under a condition on the unknowns, called realizability, which corresponds to the positivity of an underlying kinetic distribution function.
The present numerical approach is applicable to non-linear systems which possess no hyperbolic operator, and it preserves the realizability property. However the discrete equations are non-linear and we propose a numerical method to solve such non-linear systems.
Our approach is tested on academic and practical cases in 1D, 2D and 3D and it is shown to require significantly less computational power than reference methods.

AMS subject classifications: 35A35, 65M22, 35L65, 82C40

Key words: Implicit scheme, Relaxation scheme, M_1 model, Radiotherapy dose computation

1 Introduction

The present work aims to construct a numerical solver for systems of steady transport equations emerging in the field of radiotherapy. It is a follow-up to ([5, 22, 52]) and it analyses the numerical methods used [6, 14, 48–51, 53].

*Corresponding author. *Email addresses:* pichard@ljll.math.upmc.fr (T. Pichard)

The motion of energetic particles in radiotherapy can be modeled by a system of coupled linear kinetic equations over the fluences of the particles, *i.e.* over the densities, or distribution functions, of the particles in a phase space composed of position $x \in \mathbb{R}^3$, energy $\epsilon \in \mathbb{R}^+$ and direction of flight $\Omega \in \mathcal{S}^2$ on the unit sphere. Due to the high dimensionality of the phase space, solving directly such systems of equations, through either Monte Carlo methods ([15, 32, 35]) or discrete ordinates methods ([41]; see also [42] and references therein for a review on numerical approaches for dose computation) commonly requires much higher numerical powers than the standard available in medical centers. Recent technological advances lead to the development of industrial codes based on those methods which require considerably lower computational power, *i.e.* the so-called fast Monte Carlo methods (see *e.g.* [62]) and Acuros® code ([25, 46, 60]).

As an alternative in this paper, an angular moment extraction technique is used. The resulting system is underdetermined and an entropy minimization procedure is used, leading to the so-called M_1 model. Such a closure was preferred as it is known to preserve the main features of the underlying kinetic model (especially positivity, hyperbolicity and entropy dissipation), and it models accurately beams of particles. This method was widely used for diverse applications in physics and biology *e.g.* in astrophysics ([16, 17, 28]), radiative transfer ([20, 54]), in fluid dynamics ([27, 40, 43]), for semi-conductors ([29, 55]) or chemotaxis ([7]) modeling, and showed a considerable reduction of the numerical costs.

Numerical approaches for solving moment equations are typically constrained by a stability condition. Such a condition becomes very restrictive when considering low density media. Typically, the step size (see [5, 52] or Section 3 below) needs to be taken proportional to the minimum density in the medium and therefore many steps are required. This problem was first studied for application in radiotherapy in [5] and it was circumvented by the use of a clever change of variables. The previous work [52] showed another approach based on a relaxation method (based on [1,11,45], see also recent work [18]) and on the method of characteristics. However, both those approaches are inappropriate to model the motion of photons. Indeed, those numerical schemes are applicable only to hyperbolic systems, but the transport of photons was shown to be ill-modeled by such equations ([47]).

In the present paper, an implicit scheme is presented, based on a relaxation method, preserving the realizability property and efficient with large steps. However the discretized equations are non-linear and an iterative solver is constructed to solve such equations.

The paper is constructed as follows. In the next section, models of transport of photons and electrons are presented, first a kinetic model, then the angular moment extraction is described. A first numerical scheme is described for 1D problems in Section 3, an iterative algorithm adapted to this scheme is constructed and tested on an academic test case. This numerical scheme is completed and adapted to multi-D problems in Section 4 and tested on academic test cases in 2D and 3D. Section 5 is devoted to conclusion.

2 Models of transport of photons and electrons

Photons and electrons are characterized their position $x \in \mathbb{R}^3$, their energy $\epsilon \in \mathbb{R}^+$ and their direction of flight $\Omega \in \mathcal{S}^2$ on the unit sphere. The transported particles are assumed to interact only with the atoms of the background medium. The influence of such interactions on the medium are neglected. In particular, the density of atoms in the medium is given constant data.

2.1 A kinetic model

The motion of transported photons γ and electrons e is modeled by their fluence ψ_γ and ψ_e, *i.e.* their density in the (x,ϵ,Ω) space. The fluences satisfy the following steady kinetic equations (see *e.g.* [24, 32])

$$\begin{aligned} \Omega.\nabla_x \psi_\gamma(x,\epsilon,\Omega) &= \rho(x)\left[Q_{\gamma\to\gamma}(\psi_\gamma)(x,\epsilon,\Omega)+Q_{e\to\gamma}(\psi_e)(x,\epsilon,\Omega)\right], && \text{(2.1a)} \\ \Omega.\nabla_x \psi_e(x,\epsilon,\Omega) &= \rho(x)\left[Q_{e\to e}(\psi_e)(x,\epsilon,\Omega)+Q_{\gamma\to e}(\psi_\gamma)(x,\epsilon,\Omega)\right], && \text{(2.1b)} \end{aligned}$$

composed of time-independent free transport terms on the left-hand side and collisions operators on the right-hand side. The collision operator $Q_{\alpha\to\beta}$ models the variations of the fluence ψ_β due to the collisions involving incident particles α. As a first approximation, the influence of the composition of the medium on the collisions is neglected. The collision operator is only chosen to be proportional to the relative density $\rho > 0$ compared to the density of water.

The considered collision operators are given by

$$\begin{aligned} Q_{\gamma\to\gamma}(\psi_\gamma) &= [G_{\gamma\to\gamma}-P_\gamma](\psi_\gamma), && \text{(2.2a)} \\ Q_{\gamma\to e}(\psi_\gamma) &= G_{\gamma\to e}(\psi_\gamma), && \text{(2.2b)} \\ Q_{e\to\gamma}(\psi_e) &= 0, && \text{(2.2c)} \\ Q_{e\to e}(\psi_e) &= \partial_\epsilon(S\psi_e)+[G_{e\to e}-P_e](\psi_e), && \text{(2.2d)} \end{aligned}$$

where the terms $G_{\alpha\to\beta}$ and P_β are linear Boltzmann gain and loss terms given by

$$\begin{aligned} G_{\alpha\to\beta}(\psi_\alpha)(x,\epsilon,\Omega) &= \int_\epsilon^{\epsilon_{\max}} \int_{\mathcal{S}^2} \sigma_{\alpha\to\beta}(\epsilon',\epsilon,\Omega'.\Omega)\psi_\alpha(x,\epsilon',\Omega')d\epsilon' d\Omega', && \text{(2.2e)} \\ P_\beta(\psi_\beta)(x,\epsilon,\Omega) &= \sigma_{T,\beta}(\epsilon)\psi_\beta(x,\epsilon,\Omega). && \text{(2.2f)} \end{aligned}$$

The stopping power $S > 0$, the differential cross sections $\sigma_{\alpha\to\beta} \geq 0$ and the total cross sections $\sigma_{T,\beta} > 0$ are *a priori* given functions characterizing the collisions in a medium. As we have assumed that the composition of the medium did not influence the collision behaviour, the coefficients S, $\sigma_{T,\beta}$ and $\sigma_{\alpha\to\beta}$ do not depend on position x. Only the density ρ in front of the collision operators in (2.1) depends on x. Those collision operators (2.2) were chosen because they accurately model Compton, Møller, and elastic nuclear

scattering (see *e.g.* [24,32]) which are the predominant effects at the considered ranges of energy.

In medical physics, the function of interest is the energy deposited by the particles per mass unit, so-called dose. At the kinetic level, this dose D is simply given by

$$D(x)=\int_{\epsilon_{\min}}^{\epsilon_{\max}}\int_{\mathcal{S}^2}(-\epsilon)\sum_{\alpha,\beta=\gamma,e}Q_{\alpha\to\beta}(\psi_\alpha)(x,\epsilon,\Omega)d\Omega d\epsilon. \tag{2.3}$$

2.2 A moment model

Solving numerically kinetic equations of the form (2.1-2.2) requires high computational power. Instead, the method of moments is used as it requires lower computational power (see *e.g.* comparisons in the previous work [49,51,52]).

In the following, the construction of the M_1 model associated to the kinetic model (2.1-2.2) is recalled.

The moments ψ^0, ψ^1 and ψ^2 of a fluence ψ are defined by

$$\psi^0(x,\epsilon)=\int_{\mathcal{S}^2}\psi(x,\epsilon,\Omega)d\Omega,\qquad \psi^1(x,\epsilon)=\int_{\mathcal{S}^2}\Omega\psi(x,\epsilon,\Omega)d\Omega, \tag{2.4}$$
$$\psi^2(x,\epsilon)=\int_{\mathcal{S}^2}\Omega\otimes\Omega\psi(x,\epsilon,\Omega)d\Omega.$$

Extracting the moments of (2.1) up to order 1 yields, for $i=0,1$,

$$\nabla_x.\psi_\gamma^{i+1}(x,\epsilon) = \rho(x)\left[Q^i_{\gamma\to\gamma}(\psi^i_\gamma)+Q^i_{e\to\gamma}(\psi^i_e)\right](x,\epsilon), \tag{2.5a}$$
$$\nabla_x.\psi_e^{i+1}(x,\epsilon) = \rho(x)\left[Q^i_{e\to e}(\psi^i_e)+Q^i_{\gamma\to e}(\psi^i_\gamma)\right](x,\epsilon), \tag{2.5b}$$

and the moments of the collision operators of order i are

$$Q^i_{\gamma\to\gamma}(\psi_\gamma) = \left[G^i_{\gamma\to\gamma}-P^i_\gamma\right](\psi^i_\gamma), \tag{2.5c}$$
$$Q^i_{\gamma\to e}(\psi_\gamma) = G^i_{\gamma\to e}(\psi^i_\gamma), \tag{2.5d}$$
$$Q^i_{e\to\gamma}(\psi_e) = 0, \tag{2.5e}$$
$$Q^i_{e\to e}(\psi_e) = \partial_\epsilon(S\psi^i_e)+\left[G^i_{e\to e}-P^i_e\right](\psi^i_e), \tag{2.5f}$$

where the terms $G^i_{\alpha\to\beta}$ and P^i_β read

$$G^i_{\alpha\to\beta}(\psi^i_\alpha)(x,\epsilon) = \int_\epsilon^{\epsilon_{\max}}\sigma^i_{\alpha\to\beta}(\epsilon',\epsilon)\psi^i_\alpha(x,\epsilon')d\epsilon', \tag{2.5g}$$
$$P^i_\beta(\psi^i_\beta)(x,\epsilon) = \sigma_{T,\beta}(\epsilon)\psi^i_\beta(x,\epsilon), \tag{2.5h}$$
$$\sigma^i_{\alpha\to\beta}(\epsilon',\epsilon) = 2\pi\int_{-1}^{+1}\mu^i\sigma_{\alpha\to\beta}(\epsilon',\epsilon,\mu)d\mu. \tag{2.5i}$$

Remark 2.1. The value of the fluences ψ_γ and ψ_e at all energy $\epsilon' \in [\epsilon, \epsilon_{max}]$ is required to compute the integrals in the collision operators (2.5g) at energy ϵ. In practice, the equations are solved from a maximum energy ϵ_{max} to a minimum energy ϵ_{min}.

The system (2.5) is underdetermined and one more relation, so-called M_1 closure ([40, 44]), is added to close the system. This relation expresses ψ^2_α as a function of ψ^0_α and ψ^1_α for $\alpha = \gamma, e$. The M_1 closure consists in reconstructing the unique function ([8–10,30,31,40,57]) of the form

$$\psi_{M_1}(\Omega) = \exp(\boldsymbol{\lambda}.\mathbf{m}(\Omega)), \qquad \mathbf{m}(\Omega) = (1, \Omega_1, \Omega_2, \Omega_3), \qquad \boldsymbol{\lambda} = (\lambda_0, \lambda_1, \lambda_2, \lambda_3), \tag{2.6}$$

i.e. by computing the unique vector $\boldsymbol{\lambda} \in \mathbb{R}^4$ such that

$$\int_{\mathcal{S}^2} \psi_{M_1}(\Omega) d\Omega = \psi^0, \qquad \int_{\mathcal{S}^2} \Omega \psi_{M_1}(\Omega) d\Omega = \psi^1. \tag{2.7}$$

Then the last moment ψ^2 is expressed as

$$\psi^2 = \int_{\mathcal{S}^2} \Omega \otimes \Omega \psi_{M_1}(\Omega) d\Omega. \tag{2.8}$$

Using (2.6), the closure (2.8) can be rewritten (see *e.g.* [39,51])

$$\begin{aligned} \psi^2 &= \psi^0 \left(\frac{1-\chi}{2} Id + \frac{3\chi - 1}{2} \frac{\psi^1 \otimes \psi^1}{|\psi^1|^2} \right), \\ \chi &= 1 + \frac{2}{|\alpha|}(1 + \coth(|\alpha|)), \qquad \alpha = \sqrt{\lambda_1^2 + \lambda_2^2 + \lambda_3^2}, \end{aligned} \tag{2.9}$$

where χ is a scalar called Eddington factor depending on one unique scalar α. Using (2.6) and (2.7), one computes

$$\frac{|\psi^1|}{\psi^0} = \frac{|\alpha| \coth(|\alpha|) - 1}{|\alpha|}.$$

which can be inverted to compute α and therefore to obtain the closure (2.9).

Definition 2.1. The M_1 closure is defined only if there exists a function of the form (2.6) satisfying (2.7). Let us define the following set $\mathcal{R}$ called the realizability domain ([34])

$$(\psi^0, \psi^1) \in \mathcal{R} = \left\{ (f^0, f^1) \in \mathbb{R}^4, \quad \text{s.t.} \quad |f^1| \leq f^0 \right\} \cup (0, 0_{\mathbb{R}^3}). \tag{2.10}$$

The realizability domain $\mathcal{R}$ is the closure set in $\mathbb{R}^4$ of the moments of the functions of the form (2.6). It was shown that the moments of all non-negative integrable functions ([8–10]) and measures ([19,34]) belonged to the set $\mathcal{R}$.

The requirement (2.10) needs to be kept in mind when constructing numerical schemes because the flux in (2.5) becomes ill-defined if this property is violated. In particular, in the next section, the following remark is used to proof that a numerical scheme preserves the realizability property.

Remark 2.2. The realizability domain is a convex cone. Therefore, any scheme constructed based on a positive combination of realizable vector preserves the realizability property.

Since the differential cross sections $\sigma_{\alpha\to\beta}$ are also positive scalars, their moments need to satisfy the following realizability condition ([34])

$$|\sigma^1_{\alpha\to\beta}| \leq \sigma^0_{\alpha\to\beta}. \tag{2.11}$$

3 A discretization for 1D problems

We aim to construct a solver for the moment system (2.5).

For the sake of simplicity, the numerical approach is described for problems in one spatial dimension. The results are generalized to multidimensional problems in the next section.

In the first subsection, the main problem with the discretization of (2.5) is presented. A first numerical method is described and tested in the remaining subsections.

3.1 The fast characteristics problem in 1D

First the problem (2.5) is rewritten, then the main difficulty with the discretization of the rewritten equations is presented.

3.1.1 Problem settings

In 1D, the system (2.5) can be rewritten under the vectorial form

$$\partial_x \mathbf{F}(\boldsymbol{\psi})(x,\epsilon) = \rho(x)\mathbf{Q}(\boldsymbol{\psi})(x,\epsilon), \tag{3.1a}$$

where the unknown is $\boldsymbol{\psi} = (\boldsymbol{\psi}_\gamma, \boldsymbol{\psi}_e) \in \mathcal{R}^2$, and $\boldsymbol{\psi}_\alpha = (\psi^0_\alpha, \psi^1_\alpha) \in \mathcal{R}$ are the moments of the fluence of particles $\alpha = \gamma, e$. The fluxes $\mathbf{F}(\boldsymbol{\psi})$ and the collision operator $\mathbf{Q}(\boldsymbol{\psi})$ are defined over $\mathcal{R}^2$ by

$$\mathbf{F}(\boldsymbol{\psi}) = \Big(\mathbf{F}_{M_1}(\boldsymbol{\psi}_\gamma), \quad \mathbf{F}_{M_1}(\boldsymbol{\psi}_e)\Big), \tag{3.1b}$$

$$\mathbf{Q}(\boldsymbol{\psi}) = \Big(\mathbf{Q}_{\gamma\to\gamma}(\boldsymbol{\psi}_\gamma) + \mathbf{Q}_{e\to\gamma}(\boldsymbol{\psi}_e), \quad \mathbf{Q}_{e\to e}(\boldsymbol{\psi}_e) + \mathbf{Q}_{\gamma\to e}(\boldsymbol{\psi}_\gamma)\Big), \tag{3.1c}$$

and are composed of the moments of the kinetic flux and collision operator according to

$$\mathbf{F}_{M_1}(\boldsymbol{\psi}_\alpha) = (\psi^1_\alpha, \quad \psi^2_\alpha), \tag{3.1d}$$

$$\mathbf{Q}_{\alpha\to\beta}(\boldsymbol{\psi}_\alpha) = \Big(Q^0_{\alpha\to\beta}(\psi^0_\alpha), \quad Q^1_{\alpha\to\beta}(\psi^1_\alpha)\Big), \tag{3.1e}$$

where ψ_α^2 is given by the closure relation (2.8). Before describing the numerical approaches, the following notations are introduced.

Notation 1. The superscript n refers to the discretization in energy ϵ and the subscript l to the discretization in the x variable. In the next section, the subscript m will refer to the discretization in the second space variable y.

According to Remark 2.1, the energy grid is such that $\epsilon^n > \epsilon^{n+1}$.

3.1.2 Position of the problem

Standard methods to solve (3.1a) create stiff terms at the discrete level, and are therefore very time-consuming for practical applications in medical physics. Such stiffness arises in weakly collisional media, *e.g.* when the background medium has a low density ρ. This problem was illustrated in [5, 52] through a 1D electron transport equation of the form

$$\partial_x \mathbf{F}_{M_1}(\boldsymbol{\psi}_e) = \rho[\partial_\epsilon(S\boldsymbol{\psi}_e) + A\boldsymbol{\psi}_e], \qquad A = \begin{pmatrix} 0 & 0 \\ 0 & T \end{pmatrix}, \tag{3.2}$$

with $T \in \mathbb{R}^+$ by using the scheme

$$\frac{\mathbf{F}^n_{e,l+\frac{1}{2}} - \mathbf{F}^n_{e,l-\frac{1}{2}}}{\Delta x} - \rho_l \frac{S^n \boldsymbol{\psi}^n_{e,l} - S^{n+1}\boldsymbol{\psi}^{n+1}_{e,l}}{\Delta \epsilon^n} = \rho_l A^n \boldsymbol{\psi}^n_{e,l}, \tag{3.3a}$$

with numerical fluxes of Lax-Friedrichs type ([38, 58])

$$\mathbf{F}^n_{e,l+\frac{1}{2}} = \frac{1}{2}\left[\mathbf{F}_{M_1}(\boldsymbol{\psi}^n_{e,l+1}) + \mathbf{F}_{M_1}(\boldsymbol{\psi}^n_{e,l}) + (\boldsymbol{\psi}^n_{e,l+1} - \boldsymbol{\psi}^n_{e,l})\right]. \tag{3.3b}$$

Such a scheme was shown to be consistent with (3.2), however it is only stable under the following Courant-Friedrichs-Lewy (CFL) condition

$$\Delta \epsilon^n \leq S^n \Delta x \min_l(\rho_l). \tag{3.4}$$

The condition (3.4) turns very restrictive when considering low collisional media, here when ρ is small. In such a case, one requires a very large number of energy steps and therefore considerably long computational times are necessary.

A first solution to this problem was proposed in [5] by the use of a change of variable. An alternative was proposed in [52] through a method of characteristic applied on a relaxed system for (3.2). However, both methods can only be used on hyperbolic systems, and are therefore not applicable to the coupled photons-electrons transport equations (2.5).

The present discretization of the system (3.1) is presented in three parts.

- **Step 1** (Subsection 3.2): the advection operator is discretized, this corresponds to the discretization over the position variable x.

- **Step 2** (Subsection 3.3): the collision operator is discretized, this corresponds to the discretization over the energy variable ϵ.
- **Step 3** (Subsection 3.4): both discretizations are gathered to construct a numerical scheme and an iterative algorithm is constructed to solve the resulting discrete equations.

3.2 Discretization of the advection operator

In the spirit of [52], a numerical scheme for (2.5) is constructed based on the relaxation method developed in [1,11,12,45]. The principle of the relaxation method is first recalled.

The relaxation method is presented to justify the construction of the implicit scheme (3.11) below. The aim is to isolate the non-linearity in (3.1a) into a relaxation term and to solve easierly the remaining linear part by the use of an implicit scheme.

A vectorial BGK approximation of the system (2.5) is performed. In practice, the non-linear flux term is replaced by a linear advection term and a relaxation term is added the right-hand side. Let us introduce the following system of two relaxed equations

$$c^- \partial_x \mathbf{f}_\tau^- - \rho \mathbf{Q}(\mathbf{f}_\tau^-) = \frac{\mathbf{M}^- - \mathbf{f}_\tau^-}{\tau}, \tag{3.5a}$$

$$c^+ \partial_x \mathbf{f}_\tau^+ - \rho \mathbf{Q}(\mathbf{f}_\tau^+) = \frac{\mathbf{M}^+ - \mathbf{f}_\tau^+}{\tau}, \tag{3.5b}$$

where $\mathbf{f}_\tau^\pm$ are the unknowns relaxing toward the equilibrium represented by Maxwellians $\mathbf{M}^\pm(\boldsymbol{\psi}) \in \mathcal{R}^2$, and τ is a relaxation parameter. The unknowns $\mathbf{f}_\tau^\pm$ are only related to the original $\boldsymbol{\psi}$ in the limit $\tau \to 0$.

The Maxwellians $\mathbf{M}^\pm(\boldsymbol{\psi}) \in \mathcal{R}^2$ are chosen to relate to the original system through the following consistency formulae

$$\mathbf{M}^+ + \mathbf{M}^- = \boldsymbol{\psi} \in \mathcal{R}^2, \qquad c^+ \mathbf{M}^+ + c^- \mathbf{M}^- = \mathbf{F}(\boldsymbol{\psi}). \tag{3.6a}$$

The relaxation velocities $c^\pm(\boldsymbol{\psi}) \in \mathbb{R}$ are chosen such that they bound the physical velocities. This leads to the following stability requirement ([1,11,12])

$$Sp\left(\mathbf{F}'(\boldsymbol{\psi})\right) \subset [c^-, c^+]. \tag{3.7}$$

Formally, at the limit $\tau \to 0$ in (3.5), one obtains $\mathbf{f}_0^\pm = \mathbf{M}^\pm$. Then replacing $\mathbf{f}^\pm$ by $\mathbf{M}^\pm$ and summing the two equations (3.5) yields (3.1). Therefore, one recovers the solution of the original equation (3.1) in the limit case $\tau \to 0$ as

$$\boldsymbol{\psi} = \lim_{\tau \to 0} \left(\mathbf{f}_\tau^+ + \mathbf{f}_\tau^- \right). \tag{3.8}$$

We refer to [1,2,11,12,45] for a proper analysis of this asymptotic limit.

For the sake of simplicity, in the 1D case, we use the following classical result (see *e.g.* [4,13,52]), to choose the relaxation parameters.

Lemma 3.1. *The eigenvalues of the Jacobian* $\mathbf{F}'_{M_1}(\boldsymbol{\psi}_\alpha)$ *of the* M_1 *fluxes are bounded by* 1 *for all* $\boldsymbol{\psi}_\alpha \in \mathcal{R}$*, that is*

$$\forall \boldsymbol{\psi}_\alpha \in \mathcal{R}, \quad Sp(\mathbf{F}'_{M_1}(\boldsymbol{\psi}_\alpha)) \subset]-1,1[.$$

Furthermore, for all realizable moments $\boldsymbol{\psi}_\alpha \in \mathcal{R}$*, one has*

$$\boldsymbol{\psi}_\alpha \pm \mathbf{F}_{M_1}(\boldsymbol{\psi}_\alpha) \in \mathcal{R}.$$

Thus, in 1D, we will use the following parameters

$$c^+ = 1 = -c^-, \qquad \mathbf{M}^\pm = \frac{\boldsymbol{\psi} \pm \mathbf{F}(\boldsymbol{\psi})}{2} \in \mathcal{R}^2, \tag{3.9a}$$

$$\pm \partial_x \mathbf{f}_\tau^\pm - \rho \mathbf{Q}(\mathbf{f}_\tau^\pm) = \frac{\mathbf{M}^\pm - \mathbf{f}_\tau^\pm}{\tau}, \tag{3.9b}$$

which satisfy the requirements (3.6).

Then we use upwind fluxes on (3.9b) leading to the scheme

$$\frac{\mathbf{f}_{\tau,l}^{\pm,n} - \mathbf{f}_{\tau,l\mp1}^{\pm,n}}{\Delta x} - \rho \mathbf{Q}(\mathbf{f}_{\tau,l}^{\pm,n}) = \frac{\mathbf{M}^\pm - \mathbf{f}_{\tau,l}^{\pm,n}}{\tau}. \tag{3.10}$$

Then summing these equations over $\pm$ and having $\tau \to 0$ leads to define the following scheme over $\boldsymbol{\psi}$

$$\frac{\mathbf{F}^n_{l+\frac{1}{2}} - \mathbf{F}^n_{l-\frac{1}{2}}}{\Delta x} - [\rho \mathbf{Q}(\boldsymbol{\psi})]_l^n = 0, \tag{3.11a}$$

$$\mathbf{F}^n_{l+\frac{1}{2}} = \frac{1}{2}\left[\mathbf{F}(\boldsymbol{\psi}^n_{l+1}) + \mathbf{F}(\boldsymbol{\psi}^n_l) - (\boldsymbol{\psi}^n_{l+1} - \boldsymbol{\psi}^n_l)\right]. \tag{3.11b}$$

The term $[\rho \mathbf{Q}(\boldsymbol{\psi})]_l^n$ will be defined in the next subsection.

Remark 3.1. Since the collision operator $\mathbf{Q}$ is linear, one should recover

$$\mathbf{Q}(\boldsymbol{\psi})_l^n = \mathbf{Q}(\mathbf{M}^- + \mathbf{M}^+)_l^n = \mathbf{Q}(\mathbf{M}^-)_l^n + \mathbf{Q}(\mathbf{M}^+)_l^n.$$

3.3 Discretization of the collision operator

The collision terms are simply discretized with a quadrature rule for the integrals in ϵ and an implicit Euler discretization for the term $\partial_\epsilon(S\boldsymbol{\psi}_e)$. This reads

$$[\rho \mathbf{Q}(\boldsymbol{\psi})]_l^n = \rho_l \mathbf{Q}(\boldsymbol{\psi})_l^n, \tag{3.12a}$$

$$\mathbf{Q}(\boldsymbol{\psi})_l^n = \left(\mathbf{Q}_{\gamma\to\gamma}(\boldsymbol{\psi}_\gamma)_l^n + \mathbf{Q}_{e\to\gamma}(\boldsymbol{\psi}_e)_l^n, \quad \mathbf{Q}_{e\to e}(\boldsymbol{\psi}_e)_l^n + \mathbf{Q}_{\gamma\to\gamma}(\boldsymbol{\psi}_\gamma)_l^n\right), \tag{3.12b}$$

$$\mathbf{Q}_{\alpha\to\beta}(\boldsymbol{\psi}_\alpha)_l^n = \left(Q^0_{\alpha\to\beta}(\psi^0_\alpha)_l^n, \quad Q^1_{\alpha\to\beta}(\psi^1_\alpha)_l^n\right), \tag{3.12c}$$

where each discrete collision operators is, for $i=0,1$

$$Q^i_{\gamma\to\gamma}(\psi^i_\gamma)^n_l = \sum_{n'=1}^{n} \sigma^{i,n',n}_{\gamma\to\gamma}\psi^{i,n'}_{\gamma,l}\Delta\epsilon^{n'} - \sigma^n_{T,\gamma}\psi^{i,n}_{\gamma,l}, \tag{3.12d}$$

$$Q^i_{\gamma\to e}(\psi^i_\gamma)^n_l = \sum_{n'=1}^{n} \sigma^{i,n',n}_{\gamma\to e}\psi^{i,n'}_{\gamma,l}\Delta\epsilon^{n'}, \tag{3.12e}$$

$$Q^i_{e\to\gamma}(\psi^i_e)^n_l = 0, \tag{3.12f}$$

$$Q^i_{e\to e}(\psi^i_e)^n_l = \frac{S^{n-1}\psi^{i,n-1}_{e,l} - S^n\psi^{i,n}_{e,l}}{\Delta\epsilon^n} + \sum_{n'=1}^{n} \sigma^{i,n',n}_{e\to e}\psi^{i,n'}_{e,l}\Delta\epsilon^{n'} - \sigma^n_{T,e}\psi^{i,n}_{e,l}. \tag{3.12g}$$

Remark 3.2.

- We choose this particular discretization because it leads to an implicit scheme of the form (3.11-3.12), in the sense that the fluxes $\mathbf{F}^n_{l+\frac{1}{2}}$ are evaluated at the latest energy step ϵ^n. In practice, the obtained scheme is efficient even without imposing a restriction on the step size $\Delta\epsilon^n$, which circumvents the problem presented in Subsection 3.1.
- The discretization is constructed to be of order one in Δx and in $\Delta\epsilon^n$ when the solution is smooth. So the scheme (3.11-3.12) is consistent with the continuous equation (3.1a).
- In order to use the present scheme, one needs to compute $\boldsymbol{\psi}^n_l$ for all l based on $\boldsymbol{\psi}^{n'}_l$ for $n' < n$. Here, this implies solving the non-linear equation (3.11-3.12) over the vector $(\boldsymbol{\psi}^n_l)_{l=1,\dots,l_{\max}} \in (\mathcal{R}^2)^{l_{\max}}$.

3.4 An iterative solver for the 1D scheme

Writing together the discretization of the 1D advection and the collision term with the relaxation parameters (3.9) yields the following numerical scheme

$$-\mathbf{L}(\boldsymbol{\psi}^n_{l-1}) + \mathbf{D}(\boldsymbol{\psi}^n_l) - \mathbf{U}(\boldsymbol{\psi}^n_{l+1}) = \rho_l \mathbf{R}^n_l, \tag{3.13a}$$

where the operators $\mathbf{L}$ and $\mathbf{U}$ are non-linear and $\mathbf{D}$ is linear and invertible. Those operators are given by

$$\mathbf{L}(\boldsymbol{\psi}^n_{l-1}) = \frac{\boldsymbol{\psi}^n_{l-1} + \mathbf{F}(\boldsymbol{\psi}^n_{l-1})}{2\Delta x}, \qquad \mathbf{U}(\boldsymbol{\psi}^n_{l+1}) = \frac{\boldsymbol{\psi}^n_{l+1} - \mathbf{F}(\boldsymbol{\psi}^n_{l+1})}{2\Delta x}, \tag{3.13b}$$

$$\mathbf{D}(\boldsymbol{\psi}^n_l) = \left(\frac{Id}{\Delta x} + \rho_l A^n\right)\boldsymbol{\psi}^n_l, \tag{3.13c}$$

and the matrix A^n and the source $\mathbf{R}^n_l$ are given by

$$A^n\boldsymbol{\psi}^n_l = (B^n_0\boldsymbol{\psi}^n_l, \quad B^n_1\boldsymbol{\psi}^n_l, \quad D^n_0\boldsymbol{\psi}^n_l, \quad D^n_1\boldsymbol{\psi}^n_l), \tag{3.13d}$$

$$\mathbf{R}^n_l = (C^n_0, \quad C^n_1, \quad E^n_0, \quad E^n_1) + BC^n_l, \tag{3.13e}$$

with, for $i=0,1$,

$$B_i^n \boldsymbol{\psi}_l^n = (\sigma_{T,\gamma}^n - \sigma_{\gamma\to\gamma}^{i,n,n}\Delta\epsilon^n)\psi_{\gamma,l}^{i,n}, \qquad C_i^n = \sum_{n'=1}^{n-1} \sigma_{\gamma\to\gamma}^{i,n',n}\psi_{\gamma,l}^{i,n'}\Delta\epsilon^{n'}, \tag{3.13f}$$

$$D_i^n \boldsymbol{\psi}_l^n = \left(\frac{S^n}{\Delta\epsilon^n} + \sigma_{T,e}^n - \sigma_{e\to e}^{i,n,n}\Delta\epsilon^n\right)\psi_{e,l}^{i,n} - \sigma_{\gamma\to e}^{i,n,n}\psi_{\gamma,l}^{i,n}\Delta\epsilon^n, \tag{3.13g}$$

$$E_i^n = \frac{S^{n-1}}{\Delta\epsilon^n}\psi_{e,l}^{i,n-1} + \sum_{n'=1}^{n-1}\left(\sigma_{\gamma\to\gamma}^{i,n',n}\psi_{\gamma,l}^{i,n'} + \sigma_{e\to e}^{i,n',n}\psi_{e,l}^{i,n'}\right)\Delta\epsilon^{n'}. \tag{3.13h}$$

Defining properly boundary conditions for moment models based on the underlying kinetic ones remains an open problem (see *e.g.* [26, 36, 56] for linear moment equations). For the sake of simplicity, we use here discrete boundary conditions defined as a source term in (3.13e) with

$$BC_l^n = \boldsymbol{\psi}_0^n \delta_{1,l} + \boldsymbol{\psi}_{l_{\max}+1}^n \delta_{l_{\max},l},$$

with given $\boldsymbol{\psi}_0^n \in \mathcal{R}^2$ and $\boldsymbol{\psi}_{l_{\max}+1}^n \in \mathcal{R}^2$.

In order to use this scheme, one needs to solve (3.13) at each energy step n, which is a non-linear equation on the vector $(\boldsymbol{\psi}^n)_{l=1,\dots,l_{\max}}$. For this purpose, we propose an iterative solver inspired of [21], which was tested in [6, 48, 50, 51, 53].

Algorithm 1. *Initialization:* At energy step n, set $\boldsymbol{\psi}_l^{n,(0)} = \boldsymbol{\psi}_l^{n-1}$ for all l.
Iteration: Compute iteratively

$$\boldsymbol{\psi}_l^{n,(k+1)} = \mathbf{D}^{-1}\left(\mathbf{L}(\boldsymbol{\psi}_{l-1}^{n,(k)}) + \mathbf{U}(\boldsymbol{\psi}_{l+1}^{n,(k)}) + \rho_l \mathbf{R}_l^n\right), \tag{3.14}$$

until convergence.

Proposition 3.1. Suppose that $\mathbf{R}_l^n \in \mathcal{R}^2$ is realizable for all l, and that

$$\min_l \rho_l \Delta x m_A^n > \sup_{\boldsymbol{\psi}\in\mathcal{R}^2}\left(\frac{(M_F - m_F)(\boldsymbol{\psi})}{2}\right), \tag{3.15}$$

where

$$m_A^n = \min\ Sp(A^n), \quad m_F(\boldsymbol{\psi}) = \min\ Sp(\mathbf{F}'(\boldsymbol{\psi})), \quad M_F(\boldsymbol{\psi}) = \max\ Sp(\mathbf{F}'(\boldsymbol{\psi}))$$

are respectively the minimum eigenvalue of the matrix A^n, of the Jacobian $\mathbf{F}'(\boldsymbol{\psi})$ and the maximum eigenvalue of $\mathbf{F}'(\boldsymbol{\psi})$.
Then there exists a unique solution $(\boldsymbol{\psi}^n)_{l=1,\dots,l_{\max}} \in (\mathcal{R}^2)^{l_{\max}}$ satisfying (3.13) for all l. Moreover, Algorithm 1 converges to this solution.

Proof. Define the operator J over $\boldsymbol{\psi} \in (\mathcal{R}^2)^{l_{\max}}$ by

$$\boldsymbol{\psi}^{n,(k+1)} = J(\boldsymbol{\psi}^{n,(k)}),$$

where the l-th component $J(\boldsymbol{\psi}^{n,(k+1)})_l$ is given by (3.14), that is

$$J(\boldsymbol{\psi}^{n,(k+1)})_l = \left(\frac{Id}{\Delta x}+\rho_l A^n\right)^{-1}\left[\rho_l \mathbf{R}_l^n + \frac{\boldsymbol{\psi}_{l+1}^{n,(k)}-\mathbf{F}(\boldsymbol{\psi}_{l+1}^{n,(k)})}{2\Delta x}+\frac{\boldsymbol{\psi}_{l-1}^{n,(k)}+\mathbf{F}(\boldsymbol{\psi}_{l-1}^{n,(k)})}{2\Delta x}\right]. \quad (3.16)$$

First, we verify that J preserves the realizability from one step to another.

Let us suppose $\boldsymbol{\psi}^{n,(k)} \in (\mathcal{R}^2)^{l_{max}}$. Then $\boldsymbol{\psi}_{l+1}^{n,(k)} - \mathbf{F}(\boldsymbol{\psi}_{l+1}^{n,(k)}) \in \mathcal{R}^2$ and $\boldsymbol{\psi}_{l-1}^{n,(k)} + \mathbf{F}(\boldsymbol{\psi}_{l-1}^{n,(k)}) \in \mathcal{R}^2$ are realizable according to the second part of Lemma 3.1. Thus the term between square brackets in (3.16) is realizable according to Remark 2.2.

Now, we need to prove that the operator $(\frac{Id}{\Delta x}+\rho_l A^n)^{-1}$ preserves the realizability property. Using its definition (3.13), the matrix A^n can be rewritten

$$A^n = \begin{pmatrix} a_0 & 0 & 0 & 0 \\ 0 & a_1 & 0 & 0 \\ b_0 & 0 & c_0 & 0 \\ 0 & b_1 & 0 & c_1 \end{pmatrix}, \qquad \left(\frac{Id}{\Delta x}+\rho_l A^n\right)^{-1} = \begin{pmatrix} \alpha_0 & 0 & 0 & 0 \\ 0 & \alpha_1 & 0 & 0 \\ \beta_0 & 0 & \gamma_0 & 0 \\ 0 & \beta_1 & 0 & \gamma_1 \end{pmatrix}$$

where

$$\begin{aligned} a_i &= \sigma_{T,\gamma}^n - \sigma_{\gamma\to\gamma}^{i,n,n}\Delta\epsilon^n, & \alpha_i &= \frac{1}{\frac{1}{\Delta x}+\rho_l a_i}, \\ b_i &= -\sigma_{\gamma\to e}^{i,n,n}\Delta\epsilon^n, & \beta_i &= -\frac{b_i}{(\frac{1}{\Delta x}+\rho_l a_i)(\frac{1}{\Delta x}+\rho_l c_i)}, \\ c_i &= \frac{S^n}{\Delta\epsilon^n}+\sigma_{T,e}^n - \sigma_{e\to e}^{i,n,n}\Delta\epsilon^n, & \gamma_i &= \frac{1}{\frac{1}{\Delta x}+\rho_l c_i}. \end{aligned}$$

Using (2.11) leads to

$$0 \le a_0 \le a_1, \qquad 0 \le c_0 \le c_1 \quad \text{and} \quad -b_0 \ge -b_1 \ge 0$$

and so

$$\alpha_0 \ge \alpha_1 > 0, \qquad \beta_0 \ge \beta_1 > 0 \qquad \gamma_0 \ge \gamma_1 > 0.$$

Then one verifies that if $\boldsymbol{\psi} \in \mathcal{R}^2$, then $\left(\frac{Id}{\Delta x}+\rho_l A^n\right)^{-1}\boldsymbol{\psi}$ is a positive combination of vectors satisfying the criteria (2.10). So the operator $\left(\frac{Id}{\Delta x}+\rho_l A^n\right)^{-1}$ preserves the realizability, and J is an operator from $(\mathcal{R}^2)^{l_{\max}}$ into itself.

Now, in order to prove that Algorithm 1 converges, we prove that J is a contraction.

Derivating $J(\boldsymbol{\psi})$ according to $\boldsymbol{\psi}$ reads

$$d_{\boldsymbol{\psi}}J(\boldsymbol{\psi}) = \begin{pmatrix} 0 & J^n_{1,2} & 0 & \dots & 0 \\ J^n_{2,1} & 0 & J^n_{2,3} & 0 & \vdots \\ 0 & \ddots & \ddots & \ddots & 0 \\ \vdots & \ddots & \ddots & \ddots & J_{l_{\max}-1,l_{\max}} \\ 0 & \dots & 0 & J_{l_{\max},l_{\max}-1} & 0 \end{pmatrix}, \tag{3.17a}$$

$$J^n_{l,l-1} = \left(\frac{Id}{\Delta x}+\rho_l A^n\right)^{-1}\left(\frac{Id+\mathbf{F}'(\boldsymbol{\psi}_{l-1})}{2\Delta x}\right), \tag{3.17b}$$

$$J^n_{l,l+1} = \left(\frac{Id}{\Delta x}+\rho_l A^n\right)^{-1}\left(\frac{Id-\mathbf{F}'(\boldsymbol{\psi}_{l+1})}{2\Delta x}\right), \tag{3.17c}$$

so $d_{\boldsymbol{\psi}}J(\boldsymbol{\psi})$ is a block matrix with non-zero blocks on the super- and sub-diagonal.

Using a Gershgorin theorem for block matrices (see *e.g.* [59]) provides

$$Sp\left(d_{\boldsymbol{\psi}}J(\boldsymbol{\psi})\right) \subset [-r,r],$$

with a spectral radius satisfying

$$r \leq \max_l \frac{|||Id-\mathbf{F}'(\boldsymbol{\psi}_l)|||+|||Id+\mathbf{F}'(\boldsymbol{\psi}_l)|||}{2\Delta x \min Sp\left(\frac{Id}{\Delta x}+\rho_l A^n\right)}.$$

Using Lemma 3.1 and the fact that A^n is positive definite, one finds upper and lower bounds on the eigenvalues of $Id\pm\mathbf{F}'(\boldsymbol{\psi})$ and of $Id+\rho_l A^n\Delta x$ to find

$$r \leq \max_l \frac{1+\frac{(M_F-m_f)(\boldsymbol{\psi}_l)}{2}}{1+\rho_l m^n_A \Delta x}, \tag{3.18}$$

thus $r<1$ under condition (3.15), so J is a contraction and Algorithm 1 converges to the unique fixed point of J. □

Remark 3.3.

- The requirement (3.15) corresponds to a CFL-like condition. This condition was added here for to prove that the algorithm converges. However, the bound (3.18) used in the proof is not optimal. We have not yet found any theoretical nor experimental test case violating (3.15) that lead to a non-converging sequence $(\boldsymbol{\psi}^{n,(k)})_{k=1,\dots,\infty}$, even with very low collisional media (for small ρ_l). In the test cases below, Δx and $\Delta\epsilon^n$ do not necessarily respect the condition (3.15) and we always verify experimentally the convergence of Algorithm 1 at every step n. We refer *e.g.* to [3, 23, 33, 61] and references therein for more complete study on convergence for such algorithms.

- The iterative method proposed in Algorithm 1 can be interpreted as a Jacobi method with non-linear extradiagonal term. Similarily, Gauss-Seidel and successive over-relaxation (SOR) methods for the non-linear problem (3.13) can also be implemented. For example, the non-linear Gauss-Seidel type method consists in solving alternatively

$$\boldsymbol{\psi}_l^{n,(k+1)} = \mathbf{D}^{-1}\left(\mathbf{L}(\boldsymbol{\psi}_{l-1}^{n,(k+1)}) + \mathbf{U}(\boldsymbol{\psi}_{l+1}^{n,(k)}) + \rho_l \mathbf{R}_l^n\right), \tag{3.19a}$$

$$\boldsymbol{\psi}_l^{n,(k+1)} = \mathbf{D}^{-1}\left(\mathbf{L}(\boldsymbol{\psi}_{l-1}^{n,(k)}) + \mathbf{U}(\boldsymbol{\psi}_{l+1}^{n,(k+1)}) + \rho_l \mathbf{R}_l^n\right), \tag{3.19b}$$

  in Algorithm 1 instead of (3.14). One can easily adapt the proof of Proposition 3.1 for such algorithms.

- The convergence rate of Algorithm 1 depends on the eigenvalues of $d_{\boldsymbol{\psi}} J(\boldsymbol{\psi})$. In the computations (3.18), the worst possible convergence rate corresponds to the case where $(M_F - m_F)(\boldsymbol{\psi_l})$ has the highest value. Such highest value is obtained in the limit case of a purely anisotropic distribution (see *e.g.* computations in [4]) modeled by a fluence

$$\psi(\Omega) = K\delta(\Omega_1 - 1).$$

  Thus Algorithm 1 is slower if the expected solution of (2.1) possesses purely anisotropic region.

- Algorithm 1 is based on a fixed point theorem. One may think of using Newton's method to accelerate the convergence. Such method is unavailable here since the Jacobian $\mathbf{F}'(\boldsymbol{\psi})$ is not computed here. Only its upper bound was used in the proof of Proposition 3.1.

3.5 Numerical experiments

This subsection is devoted to study experimentally the convergence of the present method. Especially, two convergence rates are studied:

- The convergence according to the number $k_{\max}$ of iterations in Algorithm 1.

- The convergence according to the $\Delta\epsilon^n$ and Δx of the numerical scheme (3.13).

Those two convergence rates are studied through the following test case.

We consider a 1D domain $Z = [0\text{ cm}, 8\text{ cm}]$ uniformly composed of water (*i.e.* $\rho = 1$). A source of electrons is imposed as initial condition at $\epsilon_0 = 5$ MeV modeled by the initial condition

$$\psi_e(x, 5\text{ MeV}, \Omega) = K\mathbf{1}_{[3\text{ cm}, 5\text{ cm}]}(x), \qquad \psi_\gamma(x, 5\text{ MeV}, \Omega) = 0, \tag{3.20a}$$

and a zero condition flux is considered on the boundary which corresponds to extracting the moments of distributions of the form

$$\text{for} \quad \Omega_1 > 0, \qquad \psi_e(0\text{ cm},\epsilon,\Omega) = 0, \qquad \psi_\gamma(0\text{ cm},\epsilon,\Omega) = 0, \tag{3.21a}$$

$$\text{for} \quad \Omega_1 < 0, \qquad \psi_e(8\text{ cm},\epsilon,\Omega) = 0, \qquad \psi_\gamma(8\text{ cm},\epsilon,\Omega) = 0. \tag{3.21b}$$

Remark that the equations of system (2.1) are decoupled. As we impose no source of photons, and due to the considered physics, no photons are created in the system. Thus the solution of (2.1a) is simply $\psi_\gamma = 0$, and the discretization (3.13) can be simplified when considering beams of electrons only. This is no longer true when considering more complex physics, *e.g.* when taking into account Bremsstrahlung effect [37, 42].

The mesh is composed of 800 cells in x uniformly distributed. The step size $\Delta\epsilon^n$ and the grid in ϵ are chosen such that

$$\Delta\epsilon^n = 5S^n\Delta x. \tag{3.22}$$

This corresponds approximately to fixing

$$m_A^n \Delta x = 5.$$

With such a gridsize, we aim to avoid to have numerical diffusion effects depending $\Delta\epsilon^n$.

This test case is academic and aims only to study experimentally the numerical convergence rates. The converged dose normalized by its maximum value computed with Algorithm 1 is provided on Fig. 1 as an indication. For more examples with different applications in medical physics, we refer *e.g.* to [6, 48, 51, 53].

3.5.1 Convergence results of the iterative algorithm

The iterative method of Algorithm 1 requires a criterium to stop.

A first naive criterium consists in fixing the number of iterations k_{max}. This is not optimal, neither in terms of precision nor in terms of computational costs. At each energy step, the desired solution follows (3.13) for all l. Then one better stopping criterium consists in defining the residual

$$r^{n,(k)} = \max_l \left\| -\mathbf{L}(\boldsymbol{\psi}_{l-1}^{n,(k)}) + \mathbf{D}(\boldsymbol{\psi}_l^{n,(k)}) - \mathbf{U}(\boldsymbol{\psi}_{l+1}^{n,(k)}) - \rho_l \mathbf{R}_l^n \right\|_\infty, \tag{3.23}$$

and choose to stop Algorithm 1 as soon as k satisfies

$$r^{n,(k)} \leq r_{\max}. \tag{3.24}$$

Fig. 2 depicts the minimum number of iterations k required in Algorithm 1 such that the the residual $r^{n,(k)}$ satisfies the criterium (3.24) with $r_{\max}$ fixed at 1, 10^{-1} and 10^{-2}. This is represented as a function of the energy step n.

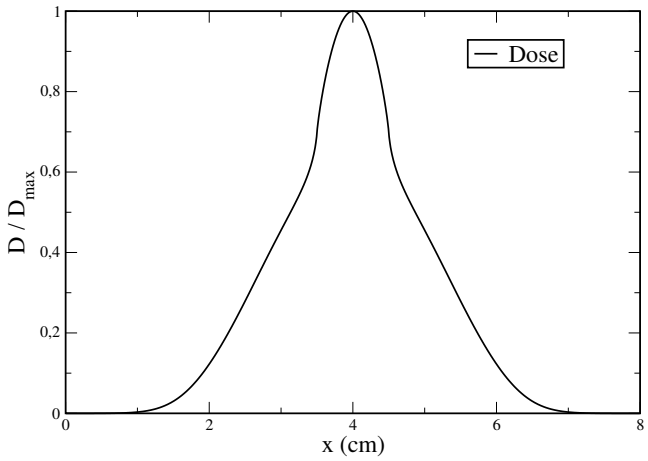

Figure 1: Normalized dose obtained with Algorithm 1 for the beam of electron (3.21).

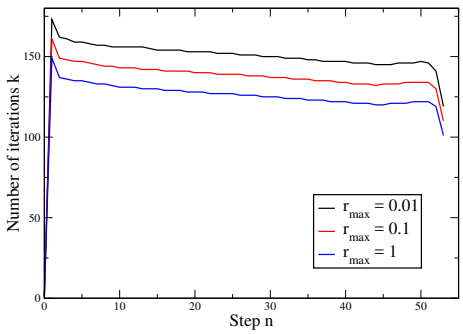

Figure 2: Number of iterations k as a function of the energy step n for a given maximum residual $r_{\max}$.

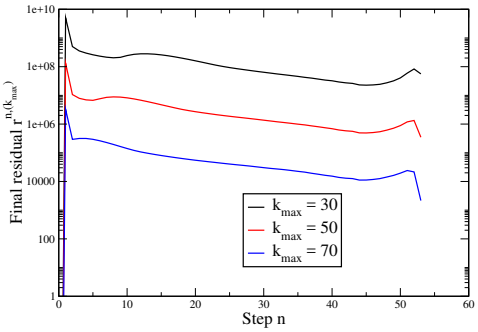

Figure 3: Final residual $r^{n,(k_{\max})}$ as a function of the energy step n for a given number of iteration $k_{\max}$.

Similarily, Fig. 3 depicts the final residual $r^{n,(k_{\max})}$ obtained by fixing $k_{\max}$ to 30, 50 or 70 as a function of the energy step n.

In the first steps where the values of ψ_e^b, Algorithm 1 requires a large number of iterations to converge. At those energy, $\partial_\epsilon \boldsymbol{\psi} \equiv (\boldsymbol{\psi}^{n-1} - \boldsymbol{\psi}^n)/\Delta\epsilon^n$ is large. Thus the intialization $\boldsymbol{\psi}^{n,(0)} = \boldsymbol{\psi}^{n-1}$ of Algorithm 1 is far from the desired solution. Therefore the present algorithm requires more iterations to converge.

The convergence rate progressively raises, *i.e.* the final residual $r^{n,(k_{\max})}$ or the number of iterations k reduce.

The drop of $r^{n,(k_{\max})}$ and of iterations k near the end of the simulation is due to the physical parameters used. The stopping power S skyrockets near the threshold $\epsilon = \epsilon_{\min}$. According to the definition of $\mathbf{D}$ in (3.13), this implies that the eigenvalues of $\mathbf{D}$ also raise

at the lowest energy. Thus the eigenvalues of J drop to zero, and so the convergence rate of Algorithm 1 skyrockets. This explains the shape of the curves k and $r^{n,(k_{\max})}$ in the last steps n.

In all the remaining test cases, the parameter $r_{\max}$ is fixed, and the parameter $k_{\max}$ is chosen sufficiently high such that the residual $r_{\max}$ is always reached during the computations, and only converged results are shown.

3.5.2 Convergence results of the numerical scheme

In this subsection, we verify experimentally that the numerical scheme is converging. The maximum residual $r_{\max}$ was fixed at 5.10^{-3}.

Since no analytical solution is known, the reference solution is chosen to be the solution obtained with the largest number of cells. The spatial domain $Z = [0,8\text{ cm}]$ is uniformly meshed. The number of spatial cells $l_{\max}$ is chosen to be 100, 200, 400, 800 and 1600 cells and for the reference solution 3200 cells. The convergence rate in Δx is represented by the discrete L^1, L^2 and L^∞ errors between the reference solution, *i.e.* the most refined one, and the less refined ones

$$\text{Error}_{L^1}(\Delta x) = \sum_{l=1}^{l_{\max}} \sum_{n=1}^{n_{\max}} \left|\boldsymbol{\psi}_l^n - \tilde{\boldsymbol{\psi}}_l^n\right| \tilde{\Delta x} \tilde{\Delta \epsilon}^n, \qquad \text{Error}_{L^2}(\Delta x) = \sqrt{\sum_{l=1}^{l_{\max}} \sum_{n=1}^{n_{\max}} (\boldsymbol{\psi}_l^n - \tilde{\boldsymbol{\psi}}_l^n)^2 \tilde{\Delta x} \tilde{\Delta \epsilon}^n},$$

$$\text{Error}_{L^\infty}(\Delta x) = \max_{l=1,\ldots,l_{\max}} \max_{n=1,\ldots,n_{\max}} \left|\boldsymbol{\psi}_l^n - \tilde{\boldsymbol{\psi}}_l^n\right|,$$

where $\boldsymbol{\psi}_l^n$ is the solution with mesh cells of size Δx and an energy step size $\Delta \epsilon^n$ given by (3.22) approximated by piecewise linear polynomials at the points (x_l, ϵ^n) on the finest mesh (of gridsize Δx) and $\tilde{\boldsymbol{\psi}}_l^n$ is the most refined solution at the same points (x_l, ϵ^n). Those errors are plotted on Fig. 4 as a function of Δx. As expected, we observe a convergence

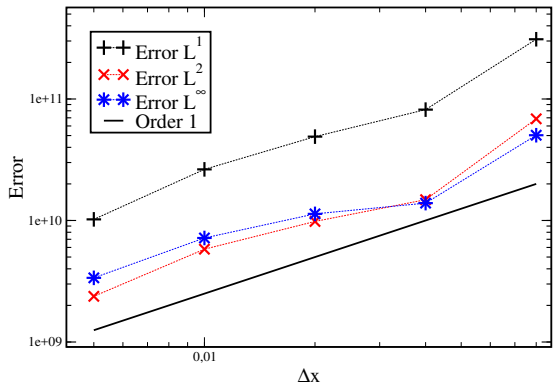

Figure 4: Discrete L^1, L^2 and L^∞ errors compared to the most refined solution as a function of Δx with $\Delta \epsilon^n$ given by (3.22).

rate of order 1, the mean slope of the curves obtained on Fig. 4 being of 1.230901 for the L^1 error, 1.213013 for the L^2 error and 0.974655 for the L^∞ error.

4 A numerical approach for multi-D problems

We extend here the previous approach for coupled electrons and photons transport in multi-D media. The difficulties and the method are described in the next three subsection in 2D through the model

$$\partial_x \mathbf{F}_1(\boldsymbol{\psi}) + \partial_y \mathbf{F}_2(\boldsymbol{\psi}) = \rho \mathbf{Q}(\boldsymbol{\psi}). \tag{4.1}$$

However the method is also valid in 3D and a 3D test case is provided in Subsection 4.4.

4.1 A correction of the numerical transverse diffusion

As described in [4, 53] and through the experimental results below, using the relaxation parameters (3.9) when considering 2D photon beams leads to a numerical overestimation of the diffusion effects in the direction orthogonal to the beams.

In multi-D, the velocities $c^\pm$ are vectors instead of scalars. We consider two relaxation velocities $c_i^\pm = \pm |c_i^\pm| e_i$ per Cartesian direction e_i. The relaxation parameters need to satisfy ([1, 11, 45])

$$\forall d \in \mathcal{S}^2, \qquad Sp\left(\mathbf{F}'_d(\boldsymbol{\psi})\right) \subset \left[\min_{i,\pm}(c_i^\pm.d),\, \max_{i,\pm}(c_i^\pm.d)\right], \tag{4.2a}$$

$$\sum_{i,\pm} \mathbf{M}_i^\pm = \boldsymbol{\psi}, \qquad \sum_{i,\pm} (c_i^\pm.d)\mathbf{M}_i^\pm = \mathbf{F}_d(\boldsymbol{\psi}), \tag{4.2b}$$

where

$$\mathbf{F}_d(\boldsymbol{\psi}) = d_1\mathbf{F}_1(\boldsymbol{\psi}) + d_2\mathbf{F}_2(\boldsymbol{\psi}) = (\psi_\gamma^1.d,\, \psi_\gamma^2.d,\, \psi_e^1.d,\, \psi_e^2.d)$$

is the flux in the direction d. In practice, we use the relaxation velocities $c_i^\pm$ defined in [53] that are assumed to approximate numerically the maximum physical velocities in each Cartesian directions

$$|c_i^\pm| \approx \max\left(\delta,\, \max\left[Sp\left(\pm \mathbf{F}'_i(\boldsymbol{\psi})\right)\right]\right).$$

Here, $\delta = 10^{-8}$ is a constant chosen arbitrarily small to avoid numerical divisions by zero. We use Maxwellians of the form

$$\mathbf{M}_i^\pm = \mu_i^\pm \boldsymbol{\psi} + \lambda_i^\pm \mathbf{F}_i(\boldsymbol{\psi}).$$

In order to satisfy (4.2b), one finds that $\mu_i^\pm$ and $\lambda_i^\pm$ need to satisfy

$$\sum_{i,\pm} \mu_i^\pm = 1, \tag{4.3a}$$

$$\lambda_i^- + \lambda_i^+ = 0, \qquad -|c_i^-|\mu_i^- + |c_i^+|\mu_i^+ = 0, \qquad -|c_i^-|\lambda_i^- + |c_i^+|\lambda_i^+ = 1. \tag{4.3b}$$

The last three equations (4.3b) can be rewritten

$$\mu_i^- = \frac{|c_i^+|}{|c_i^-|}\mu_i^+, \qquad \lambda_i^\pm = \pm\frac{1}{|c_i^+|+|c_i^-|}.$$

In practice, in 2D, we choose to fix the last degrees of freedom by

$$\mu_i^\pm = \frac{|c_i^\mp|}{2(|c_i^+|+|c_i^-|)},$$

which satisfies (4.3a). This leads to write the Maxwellians

$$\mathbf{M}_i^\pm = \frac{|\tilde{c}_i^\mp|\boldsymbol{\psi} \pm 2\mathbf{F}_i(\boldsymbol{\psi})}{2(|\tilde{c}_i^+|+|\tilde{c}_i^-|)} \in \mathcal{R}^2, \tag{4.4}$$

where $|\tilde{c}_i^\pm|$ is either $|c_i^\pm|$ or the minimum scalar such that (4.4) is realizable.

Applying the method described in Subsection 3.2 to the 2D equation (4.1) leads to write the scheme

$$\frac{\mathbf{F}^n_{l+\frac{1}{2},m}-\mathbf{F}^n_{l-\frac{1}{2},m}}{\Delta x}+\frac{\mathbf{F}^n_{l,m+\frac{1}{2}}-\mathbf{F}^n_{l,m-\frac{1}{2}}}{\Delta y}-[\rho\mathbf{Q}(\boldsymbol{\psi})]^n_{l,m}=0, \tag{4.5a}$$

$$\begin{aligned}\mathbf{F}^n_{l+\frac{1}{2},m} = {} & c^{-,n}_{l+\frac{1}{2},m}\lambda^{-,n}_{l+\frac{1}{2},m}\mathbf{F}_1(\boldsymbol{\psi}^n_{l+1,m})+c^{+,n}_{l+\frac{1}{2},m}\lambda^{+,n}_{l+\frac{1}{2},m}\mathbf{F}_1(\boldsymbol{\psi}^n_{l,m}) \\ & +\left(c^{-,n}_{l+\frac{1}{2},m}\mu^{-,n}_{l+\frac{1}{2},m}\boldsymbol{\psi}^n_{l+1,m}+c^{+,n}_{l+\frac{1}{2},m}\mu^{+,n}_{l+\frac{1}{2},m}\boldsymbol{\psi}^n_{l,m}\right),\end{aligned} \tag{4.5b}$$

$$\begin{aligned}\mathbf{F}^n_{l,m+\frac{1}{2}} = {} & c^{-,n}_{l,m+\frac{1}{2}}\lambda^{-,n}_{l,m+\frac{1}{2}}\mathbf{F}_2(\boldsymbol{\psi}^n_{l,m+1})+c^{+,n}_{l,m+\frac{1}{2}}\lambda^{+,n}_{l,m+\frac{1}{2}}\mathbf{F}_2(\boldsymbol{\psi}^n_{l,m}) \\ & +\left(c^{-,n}_{l,m+\frac{1}{2}}\mu^{-,n}_{l,m+\frac{1}{2}}\boldsymbol{\psi}^n_{l,m+1}+c^{+,n}_{l,m+\frac{1}{2}}\mu^{+,n}_{l,m+\frac{1}{2}}\boldsymbol{\psi}^n_{l,m}\right),\end{aligned} \tag{4.5c}$$

where the coefficients in the discrete fluxes are given by

$$\lambda^{\pm,n}_{j,k} = \pm\frac{1}{|c^{+,n}_{j,k}|+|c^{-,n}_{j,k}|}, \qquad \mu^{\pm,n}_{j,k} = \frac{|c^{\mp,n}_{j,k}|}{2(|c^{+,n}_{j,k}|+|c^{-,n}_{j,k}|)},$$

$$c^{\pm,n}_{l+\frac{1}{2},m} = \pm\max\left(|\tilde{c}_1^\pm(\boldsymbol{\psi}^n_{l+1,m})|,|\tilde{c}_1^\pm(\boldsymbol{\psi}^n_{l,m})|\right),$$

$$c^{\pm,n}_{l,m+\frac{1}{2}} = \pm\max\left(|\tilde{c}_2^\pm(\boldsymbol{\psi}^n_{l,m+1})|,|\tilde{c}_2^\pm(\boldsymbol{\psi}^n_{l,m})|\right),$$

for $(j,k)=(l+\frac{1}{2},m)$ or $(j,k)=(l,m+\frac{1}{2})$.

4.2 An iterative solver for the multi-D scheme with the transverse diffusion correction

We propose to adapt Algorithm 1 when the coefficients $c_i^\pm$ are not constants. In this case, the scheme (4.5) can be rewritten under the form

$$\begin{aligned}\rho_l\mathbf{R}^n_l = {} & -\mathbf{L}_1(\boldsymbol{\psi}^n_{l-1,m})-\mathbf{L}_2(\boldsymbol{\psi}^n_{l,m-1})+\mathbf{D}(\boldsymbol{\psi}^n_{l,m}) \\ & -\mathbf{U}_1(\boldsymbol{\psi}^n_{l+1,m})-\mathbf{U}_2(\boldsymbol{\psi}^n_{l,m+1}),\end{aligned} \tag{4.6a}$$

where the operators $\mathbf{L}_1$, $\mathbf{L}_2$, $\mathbf{U}_1$, $\mathbf{U}_2$ and $\mathbf{D}$ yield

$$\begin{aligned}
\mathbf{L}_1(\boldsymbol{\psi}^n_{l-1,m}) &= \frac{c^{+,n}_{l-\frac{1}{2},m}}{\Delta x}\left[\mu^{+,n}_{l-\frac{1}{2},m}\boldsymbol{\psi}^n_{l-1,m}+\lambda^{+,n}_{l-\frac{1}{2},m}\mathbf{F}_1(\boldsymbol{\psi}^n_{l-1,m})\right], && (4.6b)\\
\mathbf{L}_2(\boldsymbol{\psi}^n_{l,m-1}) &= \frac{c^{+,n}_{l,m-\frac{1}{2}}}{\Delta y}\left[\mu^{+,n}_{l,m-\frac{1}{2}}\boldsymbol{\psi}^n_{l,m-1}+\lambda^{+,n}_{l,m-\frac{1}{2}}\mathbf{F}_2(\boldsymbol{\psi}^n_{l,m-1})\right], && (4.6c)\\
\mathbf{U}_1(\boldsymbol{\psi}^n_{l+1,m}) &= \frac{-c^{-,n}_{l+\frac{1}{2},m}}{\Delta x}\left[\mu^{-,n}_{l+\frac{1}{2},m}\boldsymbol{\psi}^n_{l+1,m}+\lambda^{-,n}_{l+\frac{1}{2},m}\mathbf{F}_1(\boldsymbol{\psi}^n_{l+1,m})\right], && (4.6d)\\
\mathbf{U}_2(\boldsymbol{\psi}^n_{l,m+1}) &= \frac{-c^{-,n}_{l,m+\frac{1}{2}}}{\Delta y}\left[\mu^{-,n}_{l,m+\frac{1}{2}}\boldsymbol{\psi}^n_{l,m+1}+\lambda^{-,n}_{l,m+\frac{1}{2}}\mathbf{F}_2(\boldsymbol{\psi}^n_{l,m+1})\right], && (4.6e)\\
\mathbf{D}(\boldsymbol{\psi}^n_{l,m}) &= \left(\rho_l A^n+\beta^n_{l,m}Id\right)\boldsymbol{\psi}^n_{l,m}+\gamma^n_{1,l,m}\mathbf{F}_1(\boldsymbol{\psi}^n_{l,m})+\gamma^n_{2,l,m}\mathbf{F}_2(\boldsymbol{\psi}^n_{l,m}), && (4.6f)
\end{aligned}$$

where the coeffiecients $\beta^n_{l,m}$, $\gamma^n_{1,l,m}$ and $\gamma^n_{2,l,m}$ read

$$\begin{aligned}
\beta^n_{l,m} &= \frac{c^{+,n}_{l+\frac{1}{2},m}\mu^{+,n}_{l+\frac{1}{2},m}-c^{-,n}_{l-\frac{1}{2},m}\mu^{-,n}_{l-\frac{1}{2},m}}{\Delta x}+\frac{c^{+,n}_{l,m+\frac{1}{2}}\mu^{+,n}_{l,m+\frac{1}{2}}-c^{-,n}_{l,m-\frac{1}{2}}\mu^{-,n}_{l,m-\frac{1}{2}}}{\Delta y},\\
\gamma^n_{1,l,m} &= \frac{c^{+,n}_{l+\frac{1}{2},m}\lambda^{+,n}_{l+\frac{1}{2},m}-c^{-,n}_{l-\frac{1}{2},m}\lambda^{-,n}_{l-\frac{1}{2},m}}{\Delta x},\\
\gamma^n_{2,l,m} &= \frac{c^{+,n}_{l,m+\frac{1}{2}}\lambda^{+,n}_{l,m+\frac{1}{2}}-c^{-,n}_{l,m-\frac{1}{2}}\lambda^{-,n}_{l,m-\frac{1}{2}}}{\Delta y}.
\end{aligned}$$

The difficulty here emerges from the non-linearity of the operator $\mathbf{D}$ to invert and from the realizability requirements (4.2).

Let us decompose the operator $\mathbf{D}$ into

$$\begin{aligned}
\mathbf{D}(\boldsymbol{\psi}) &= \mathbf{D}_{imp}(\boldsymbol{\psi})-\mathbf{D}_{exp}(\boldsymbol{\psi}), && (4.7)\\
\mathbf{D}_{imp}(\boldsymbol{\psi}) &= \left[\rho_l A^n+(\alpha^n_{l,m}+\beta^n_{l,m})Id\right]\boldsymbol{\psi},\\
\mathbf{D}_{exp}(\boldsymbol{\psi}) &= \alpha^n_{l,m}\boldsymbol{\psi}+\gamma^n_{1,l,m}\mathbf{F}_1(\boldsymbol{\psi})+\gamma^n_{2,l,m}\mathbf{F}_2(\boldsymbol{\psi}),
\end{aligned}$$

such that $\mathbf{D}_{imp}$ is linear and invertible. Here the coefficient $\alpha^n_{l,m}$ is chosen non-negative such that the operator $\mathbf{D}_{exp}$ preserves the realizability. In practice, one may simply chose

$$\alpha^n_{l,m}=|\gamma^n_{1,l,m}|+|\gamma^n_{2,l,m}|.$$

Finally, Algorithm 1 is rewritten by modifying (3.14). This leads to the following algorithm.

Algorithm 2. *Initialization:* Set $\boldsymbol{\psi}^{n,(0)}_{l,m}=\boldsymbol{\psi}^{n-1}_{l,m}$ for all l,m.
Iteration: Compute iteratively

$$\begin{aligned}
\boldsymbol{\psi}^{n+1,(k+1)}_{l,m} &= \mathbf{D}^{-1}_{imp}\Big(\mathbf{R}^n_{l,m}+\mathbf{L}_1(\boldsymbol{\psi}^{n+1,(k)}_{l-1,m})+\mathbf{L}_2(\boldsymbol{\psi}^{n+1,(k)}_{l,m-1}) && (4.8)\\
&\qquad +\mathbf{D}_{exp}(\boldsymbol{\psi}^{n+1,(k)}_{l,m})+\mathbf{R}_1(\boldsymbol{\psi}^{n+1,(k)}_{l-1,m})+\mathbf{R}_2(\boldsymbol{\psi}^{n+1,(k)}_{l,m-1})\Big),
\end{aligned}$$

until convergence.

Remark 4.1.

- The parameter $\alpha^n Id$ was artificially added on both sides of (4.7) when splitting the operator $\mathbf{D}$ in two parts. This enforces the preservation of the realizability property and makes the algorithm more stable. However, this reduces the convergence rate of Algorithm 2.
- One may reproduce the computations from the proof of Proposition 3.1 with (4.8) to show that the realizability property is preserved from one iteration to another in Algorithm 2 and to show it is convergent.

4.3 Numerical experiment in 2D: a photon beam in water

In this test case, photons are injected in a 2D homogeneous domain composed of water. The size of the medium is 2 cm $\times$ 10 cm, and a 0.5 cm large beam of 500 keV photons is injected on the left boundary. This is modeled by the following incoming boundary condition

$$\begin{aligned}
\text{for} \quad (X,\Omega)\in\Gamma^- &= \left\{(X,\Omega)\in\partial Z\times\mathcal{S}^2 \quad \text{s.t.} \quad n(X).\Omega<0\right\},\\
\psi_\gamma(X,\epsilon,\Omega) &= 10^{10}\exp\left(-\alpha_\epsilon(\epsilon-\epsilon_0)^2\right)\exp\left(-\alpha_\mu(\Omega_1-1)^2\right)\mathbf{1}_B(X)+\delta\mathbf{1}_{\partial Z\setminus B}(X),\\
\psi_e(X,\epsilon,\Omega) &= \delta,\\
B &= \left\{(x,y), \quad x=0, \quad y\in[0.75\text{ cm},1.25\text{ cm}]\right\},
\end{aligned}$$

where $n(X)$ is the outgoing normal, $\epsilon_0=500$ keV, $\alpha_\epsilon=20000$, $\alpha_\mu=500000$ and $\delta=10^{-15}$. And we used the moments of those distribution as boundary conditions for the moment equations.

Through this test case, we aim to highlight the influence of the choice of the parameters $c^\pm$ on the convergence rate of Algorithm 1. The influence of $c^\pm$ on the dose results were studied in [53] and are only recalled here for completeness. The present method is tested using two sets of parameters $c_i^\pm$:

- First, we fix $|c_i^\pm|=2$ at a sufficiently large value (afterward called large c) for the conditions (4.2) to be satisfied. Those parameters were shown to provide an overestimated numerical angular diffusion in [53] (see also Fig. 5 below).
- Second, we fix $c_i^\pm$ at a value closer to the value actual eigenvalues of the Jacobian of the flux as proposed in [53] (afterward called small c). These parameters were shown to reduce the diffusion effects of the numerical method, especially in the direction orthogonal to the beam.

Algorithm 2 is compared to a reference Monte Carlo solver ([24]). The dose results obtained with those methods are gathered on Fig. 5 with the computational times in Table

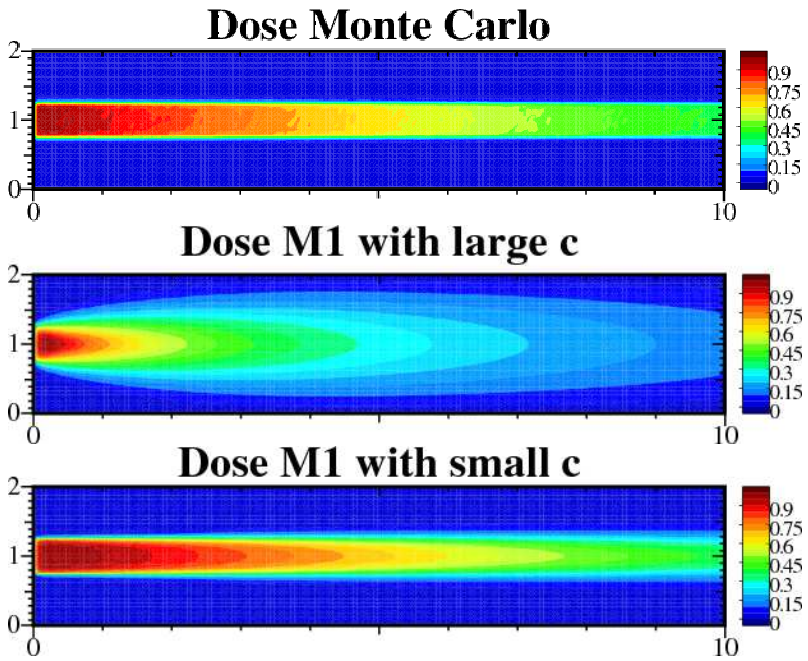

Figure 5: Doses obtained with the Monte Carlo solver (top) and the M_1 solver with large c (middle) and small c (below) relaxation parameters, normalized by their maximum value.

Solver	Monte Carlo	M_1 with large c	M_1 with small c
Computation times	14 hours	49.78699 sec	204.1239 sec

Table 1: Computational times with the Monte Carlo solver and the implicit solver with the different c.

1. A cut of the doses along the axis of the beam $y=1$ cm and in the transverse direction at depth $x=2$ cm and $x=8$ cm are shown on Fig. 6.

The dose results with the modified relaxation parameters are much closer to the reference Monte Carlo results. As expected the dose is less diffused with the small c.

Due to the noise in the Monte Carlo and the normalization by $\max D$, the M_1 dose curves with the modified relaxation parameters are slightly above the Monte Carlo reference on Fig. 6.

Following Remark 4.1, we observe that the computational time is higher with the small c than with the large ones. Those times remains much lower than the one with the Monte Carlo reference.

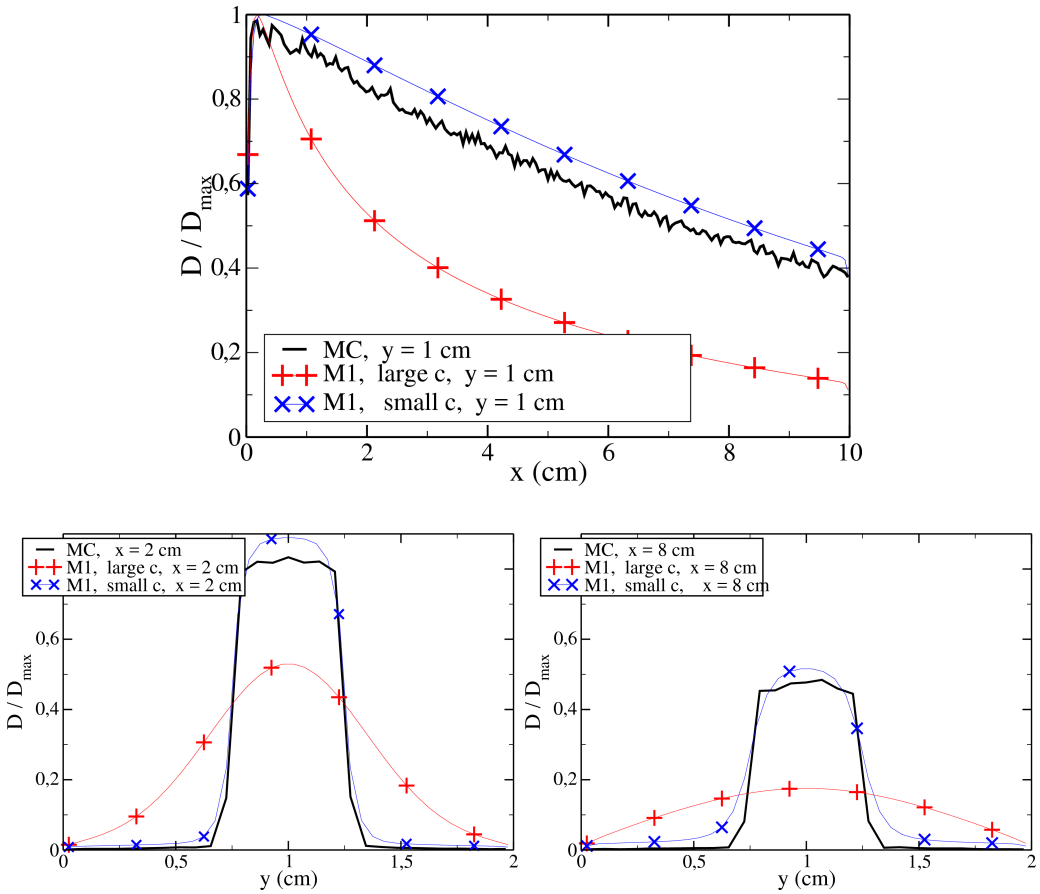

Figure 6: Doses obtained with the Monte Carlo solver and the M_1 solver with large and small c along the axis of the beam (top) and the axis transverse to the beam at 2 cm depth (below left) and 8 cm depth (below right), normalized by their maximum value.

4.4 Numerical experiment in 3D: a photon beam in a chest

This test case aims to exhibit the efficiency of our method when considering more complex density maps. For this purpose, a density map obtained from a computed tomography (CT) scan of a chest is used. This map is depicted on Fig. 7. This domain is a 29.5 cm deep cube.

A beam of photons is imposed on the boundary of the medium to pass through the ribs. In order to reduce the computational time, the computations are performed on a smaller domain of size 14 cm $\times$ 25 cm $\times$ 11.35 cm in which the density of photons is non-negligible. This domain is meshed with $140 \times 220 \times 50$ cells.

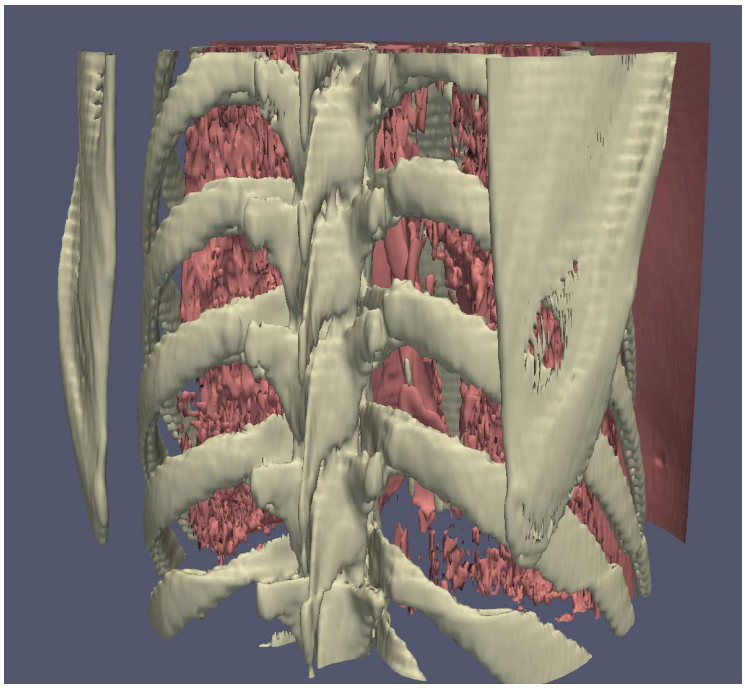

Figure 7: Density map represented by isosurfaces of density 1.8 (ivory; equivals to bone density) and 0.3 (flesh colour; equivals to lung density).

The beam is modeled by the following condition over Γ^-

$$\begin{aligned}\psi_\gamma(X,\epsilon,\Omega) &= 10^{10}\exp\left(-\alpha_\epsilon(\epsilon-\epsilon_0)^2\right)\exp\left(-\alpha_\mu(\Omega_2-1)^2\right)\mathbf{1}_B(X)+\delta\mathbf{1}_{\partial Z\setminus B}(X),\\ \psi_e(X,\epsilon,\Omega) &= \delta,\end{aligned}$$

$$B=\left\{(x,y,z),\quad x\in[6\text{ cm},8\text{ cm}],\ y=0\text{ cm},\ z\in[4\text{ cm},6\text{ cm}]\right\},$$

where $n(x)$ is the outgoing normal, $\epsilon_0=1$ MeV, $\alpha_\epsilon=20000$, $\alpha_\mu=3000$ and $\delta=10^{-15}$. And we used the moments of those distribution as boundary conditions for the moment equations.

The maximum residual was fixed at $r_{\max}=10^{-1}$.

The computations were performed with the small parameters c. Those dose results are depicted on Fig. 8 as isodose surfaces cut along the surfaces parametrized by $\{x=5$ cm$\}$, $\{y=12.5$ cm$\}$ and $\{z=5.675$ cm$\}$, that are along the axis of the beam or at half depth in the domain.

The present method was tested on a rather complex problem with a large 3D mesh, a complete physics (photons and electrons together) and using the large c, that is in the most complex settings. The computations were performed in parallel on four cores and the computational times are gathered in Table 2. These times of computataion remains

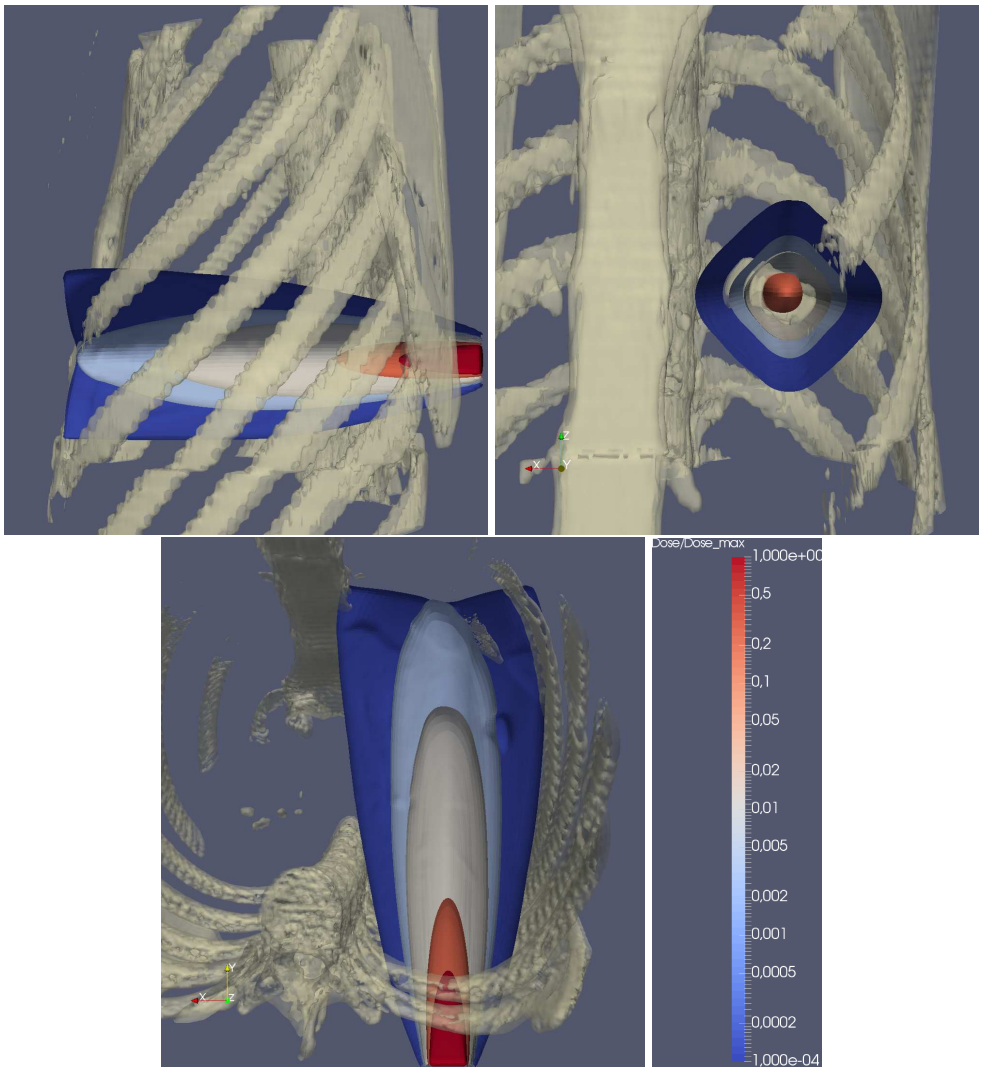

Figure 8: Isosurfaces of dose at 60%, 30%, 6%, 3% and 0.6% of the maximum dose in a chest.

Solver	M_1 with small c
Computation times	10405 sec $\approx$ 2 h 53 min

Table 2: Computational times with the implicit solver for the 3D problem.

too long for practical applications in medical physics. Several features in our approach can be improved to reduce drastically the computational times. The main time consuming issue and an axe of improvement are presented here.

In practice, the moments $\boldsymbol{\psi}$ are computed in the whole space-energy domain, even in cells where they are negligible. This results in solving (4.8) over a very large vector $\boldsymbol{\psi}^n$. Those non-necessary computations raise the size of the system to solve and reduce the convergence rate of our algorithm (see Remark 3.3).

The computational times can be considerably reduced using common code optimization techniques. The most common idea for such a problem is the mesh adaptation, here over the space and the energy. Instead of computing $\boldsymbol{\psi}$ in the whole domain, one may solve (4.8) on a smaller domain where $\boldsymbol{\psi}$ is expected not to be negligible. This would lead to a considerable reduction of both the computational times and the memory requirements. This method was also used in the development of the industrial code Acuros® [25, 46, 60] with considerable ressources requirement reduction.

5 Conclusions

The present approach aims to circumvent restrictive stability conditions when numerically solving coupled linear kinetic equations.

First, an angular moment extraction was performed leading to a so-called M_1 system of equations. Such models require lower computational cost to solve, but are valid under a realizability condition.

A numerical scheme for M_1 systems was proposed by chosing implicit flux and collision terms. Then an iterative method was constructed to compute the solution of such an implicit scheme. The proposed algorithm was constructed with a special focus on the preservation of the realizability property.

Numerical experiments showed that our method behaves appropriately in practical cases in 1D and in multi-D and the convegence of the method was tested in 1D. The present approach was shown to require much lower computational costs than a reference Monte Carlo method.

Acknowledgement

The authors are grateful to Gabriele Birindelli (Université de Bordeaux) and Kerstin Küpper (RWTH Aachen) for performing the PENELOPE simulations, and to Martin Frank (RWTH Aachen) for fruitful discussions. This work was partially funded by Aquitaine Region and FEDER fund through IOPRA interface. T. Pichards PhD and postdoctoral research were funded respectively by IdEx Bordeaux and Aquitaine Region; and by CEA and LJLL through LRC Manon.

References

[1] D. Aregba-Driollet and R. Natalini. Discrete kinetic schemes for multidimensional systems of conservation laws. *SIAM J. Numer. Anal.*, 6:1973–2004, 2000.

[2] D. Aregba-Driollet, R. Natalini, and S. Tang. Explicit diffusive kinetic schemes for nonlinear degenerate parabolic systems. *Math. Comp.*, 73:63–94, 2004.
[3] O. Axelsson. *Iterative solution methods*. Cambridge University Press, New York, NY, USA, 1994.
[4] C. Berthon, P. Charrier, and B. Dubroca. An HLLC scheme to solve the M_1 model of radiative transfer in two space dimensions. *J. Sci. Comput.*, 31(3):347–389, 2007.
[5] C. Berthon, M. Frank, C. Sarazin, and R. Turpault. Numerical methods for balance laws with space dependent flux: Application to radiotherapy dose calculation. *Commun. Comput. Phys.*, 10(5), 2011.
[6] G. Birindelli, J.-L. Feugeas, J. Caron, B. Dubroca, G. Kantor, J. Page, T. Pichard, V. T. Tikhonchuk, and Ph. Nicolaï. High performance modelling of the transport of energetic particles for photon radiotherapy. *Phys. Med., spec. issue SFPM 2016 conference*, to appear.
[7] R. Borsche, J. Kall, A. Klar, and T.N.H. Pham. Kinetic and related macroscopic models for chemotaxis on networks. *Math. Mod. Meth. Appl. S.*, 26(6):1219–1242, 2016.
[8] J. Borwein and A. Lewis. Duality relationships for entropy-like minimization problems. *SIAM J. Control Optim.*, 29(2):325–338, 1991.
[9] J. Borwein and A. Lewis. Partially finite convex programming, part I: Quasi relative interiors and duality theory. *Math. Program.*, 57:15–48, 1992.
[10] J. Borwein and A. Lewis. Partially finite convex programming: Part II. *Math. Program.*, 57:49–83, 1992.
[11] F. Bouchut. Construction of BGK models with a family of kinetic entropies for a given system of conservation laws. *J. Stat. Phys.*, 95(1):113–170, 1998.
[12] F. Bouchut, F. R. Guarguaglini, and R. Natalini. Diffusive BGK approximations for nonlinear multidimensional parabolic equations. *Indiana Univ. Math. J.*, 49:723–749, 2000.
[13] T. A. Brunner and J. P. Holloway. One-dimensional riemann solvers and the maximum entropy closure. *J. Quant. Spectros. Radiat. Transfer*, 69(5):543 – 566, 2001.
[14] J. Caron, J.-L. Feugeas, B. Dubroca, G. Kantor, C. Dejean, G. Birindelli, T. Pichard, Ph. Nicolaï, E. d'Humières, M. Frank, and V. Tikhonchuk. Deterministic model for the transport of energetic particles: Application in the electron radiotherapy. *Phys. Medica*, 31(8):912–921, 2015.
[15] CERN. *Geant4 user's guide for application developers*, 2015.
[16] S. Chandrasekhar. On the radiative equilibrium of a stellar atmosphere. *Astrophys. J.*, 99:180 – 190, 1943.
[17] S. Chandrasekhar. On the radiative equilibrium of a stellar atmosphere X. *Astrophys. J.*, 103:351 – 370, 1946.
[18] D. Coulette, E. Franck, P. Helluy, M. Mehrenberger, and L. Navoret. Palindromic discontinuous Galerkin method for kinetic equations with stiff relaxation. *Hal archives ouvertes*, 2016.
[19] R. Curto and L. A. Fialkow. Recusiveness, positivity, and truncated moment problems. *Houston J. Math.*, 17(4):603–634, 1991.
[20] B. Dubroca and J.-L. Feugeas. Hiérarchie des modèles aux moments pour le transfert radiatif. *C. R. Acad. Sci. Paris*, 329:915–920, 1999.
[21] B. Dubroca and M. Frank. An iterative method for transport equations in radiotherapy. *Progress in Industrial Mathematics at ECMI 2008*, pages 407–412, 2010.
[22] R. Duclous, B. Dubroca, and M. Frank. A deterministic partial differential equation model for dose calculation in electron radiotherapy. *Phys. Med. Biol.*, 55:3843–3857, 2010.
[23] L. Elsner and V. Mehrmann. Convergence of block iterative methods for linear systems arising in the numerical solution of euler equations. *Numer. Math.*, 59(1):541–559, 1991.

[24] J. Sempau F. Salvat, J. M. Fernández-Varea. *PENELOPE-2011: A code system for Monte Carlo simulation of electron and photon transport*, 2011.
[25] G.A. Failla, T.A. Wareing, Y. Archambault, and S. Thompson. Acuros XB ® advanced dose calculation for the Eclipse ™ treatement planning system. *Clinical perspectives*, 2010.
[26] B. D. Ganapol, C. T. Kelley, and G. C. Pomraning. Asymptotically exact boundary conditions for the P_N equations. *Nucl. Sci. Eng.*, 114, 1993.
[27] C. Groth and J. McDonald. Towards physically realizable and hyperbolic moment closures for kinetic theory. *Cont. Mech. Therm.*, 21(6):467–493, 2009.
[28] T. Hanawa and E. Audit. Reformulation of the M_1 model of radiative transfer. *J. Quant. Spectros. Radiat. Transfer*, 145:9 – 16, 2014.
[29] C. Hauck. *Entropy-based moment closures in semiconductor models*. PhD thesis, University of Maryland, 2006.
[30] C. D. Hauck, C. D. Levermore, and A. L. Tits. Convex duality and entropy-based moment closures: Characterizing degenerate densities. *SIAM J. Control Optim.*, 2007.
[31] M. Junk. Maximum entropy for reduced moment problems. *Math. Mod. Meth. Appl. S.*, 10(1001–1028):2000, 1998.
[32] I. Kawrakow and D. W. Rogers. *The EGSnrc code system*, 2013.
[33] C. Kelley. *Iterative methods for linear and nonlinear equations*. SIAM, 1995.
[34] D. Kershaw. Flux limiting nature's own way. Technical report, Lawrence Livermore Laboratory, 1976.
[35] Los Alamos National Laboratory. *MCNP - A general Monte Carlo N-particle transport code, Version 5*, 2003.
[36] E. W. Larsen and G. C. Pomraning. The P_N theory as an asymptotic limit of transport theory in planar geometry I: Analysis. *Nucl. Sci. Eng.*, 109(49), 1991.
[37] T. Leroy, R. Duclous, B. Dubroca, V.T. Tikhonchuk, S. Brull, A. Decoster, M. Lobet, and L. Gremillet. Deterministic and stochastic kinetic descriptions of electron-ion Bremsstrahlung: From thermal to non-thermal regimes, 2014. Project at CEMRACS.
[38] R. J. LeVeque. *Finite Volume methods for hyperbolic problems*, volume 31. Cambridge university press, 2002.
[39] C. D. Levermore. Relating eddington factors to flux limiters. *J. Quant. Spectrosc. Radiat. Transfer*, 31(2):149–160, 1984.
[40] C. D. Levermore. Moment closure hierarchies for kinetic theories. *J. Stat. Phys.*, 83(5–6):1021–1065, 1996.
[41] E. E. Lewis and W. F. Miller. *Computational methods of neutron transport*. American nuclear society, 1993.
[42] P. Mayles, A. Nahum, and J.C. Rosenwald, editors. *Handbook of radiotherapy physics: Theory and practice*. Taylor & Francis, 2007.
[43] J. Mcdonald and M. Torrilhon. Affordable robust moment closures for CFD based on the maximum-entropy hierarchy. *J. Comput. Phys.*, 251:500–523, 2013.
[44] G. N. Minerbo. Maximum entropy Eddington factors. *J. Quant. Spectros. Radiat. Transfer*, 20:541–545, 1978.
[45] R. Natalini. A discrete kinetic approximation of entropy solutions to multidimensional scalar conservation laws. *J. Differ. Equations*, 148(2):292 – 317, 1998.
[46] J. Ojala. The accuracy of acuros xb algorithm in external beam radiotherapy - a comprehensive review. Technical report.
[47] E. Olbrant and M. Frank. Generalized Fokker-Planck theory for electron and photon transport in biological tissues: Application to radiotherapy. *Comput. Math. Methods Med.*,

11(4):313–339, 2010.

[48] J. Page, J.-L. Feugeas, G. Birindelli, J. Caron, B. Dubroca, G. Kantor, T. Pichard, V.T. Tikhonchuk, and Ph. Nicolaï. New fast entropic algorithm for MRI-guided radiotherapy. *Phys. Med., spec. issue SFPM 2016 conference*, to appear.

[49] T. Pichard. *Mathematical modelling for dose deposition in photontherapy*. PhD thesis, Université de Bordeaux and RWTH Aachen University, 2016.

[50] T. Pichard, G.W. Alldredge, S. Brull, B. Dubroca, and M. Frank. The M_2 model for dose simulation in radiation therapy. *J. Comput. Theor. Transport, spec. issue ICTT 2015 conference*, 2016.

[51] T. Pichard, G.W. Alldredge, S. Brull, B. Dubroca, and M. Frank. An approximation of the M_2 closure: Application to radiotherapy dose simulation. *J. Sci. Comput*, 71(1):71–108, 2017.

[52] T. Pichard, D. Aregba-Driollet, S. Brull, B. Dubroca, and M. Frank. Relaxation schemes for the M_1 model with space-dependent flux: Application to radiotherapy dose calculation. *Commun. Comput. Phys.*, 19:168–191, 2016.

[53] T. Pichard, S. Brull, B. Dubroca, and M. Frank. On the transverse diffusion of beams of photons in radiation therapy. *Proc. HYP2016 conference*, to appear.

[54] G. C. Pomraning. *The equations of radiation hydrodynamics*. Pergamon Press, 1973.

[55] S. La Rosa, G. Mascali, and V. Romano. Exact maximum entropy closure of the hydrodynamical model for Si semiconductors: The 8-moment case. *SIAM J. Appl. Math.*, 70(3):710–734, 2009.

[56] R. P. Rulko, E. W. Larsen, and G. C. Pomraning. The P_N theory as an asymptotic limit of transport theory in planar geometry II: Numerical results. *Nucl. Sci. Eng.*, 109(76), 1991.

[57] J. Schneider. Entropic approximation in kinetic theory. *ESAIM-Math. Model. Num.*, 38(3):541–561, 2004.

[58] E. Toro. *Riemann solvers and numerical methods for fluid dynamics*. Springer, 2009.

[59] A. van der Sluis. Gershgorin domains for partitioned matrices. *Linear Algebra Appl.*, 26:265 – 280, 1979.

[60] O. N. Vassiliev, T. A. Wareing, J. McGhee, G. Failla, M. R. Salehpour, and F. Mourtada. Validation of a new grid-based Boltzmann equation solver for dose calculation in radiotherapy with photon beams. *Phys. Med. Biol.*, 55:581–598, 2010.

[61] M.N. Vrahatis, G.D. Magoulas, and V.P. Plagianakos. From linear to nonlinear iterative methods. *Appl. Numer. Math.*, 45(1):59 – 77, 2003.

[62] C. Zankowski, M. Laitinen, and H. Neuenschwander. Fast electron Monte Carlo for Eclipse^{TM}. Technical report, Varian Medical System.